Nuclear Engineering and Design 239 (2009) 2022–2034

Contents lists available at ScienceDirect

Nuclear Engineering and Design

journal homepage: www.elsevier.com/locate/nucengdes

Experimental study of the characteristics of the flow in the first rows of tube banks

Cláudio R. Olinto[a,1], Maria Luiza S. Indrusiak[a,2], Luiz Augusto M. Endres[b], Sergio V. Möller[a,*]

[a] Programa de Pós-Graduação em Engenharia Mecânica - PROMEC, Universidade Federal do Rio Grande do Sul - UFRGS, Rua Sarmento Leite, 425, CEP 90050-170, Porto Alegre, RS, Brazil
[b] Instituto de Pesquisas Hidráulicas - IPH, Universidade Federal do Rio Grande do Sul - UFRGS, Av. Bento Gonçalves, 950, CEP 91501-970, Porto Alegre, RS, Brazil

ARTICLE INFO

Article history:
Received 18 November 2008
Received in revised form 27 May 2009
Accepted 29 May 2009

ABSTRACT

This paper presents the experimental study of the flow instabilities in the first rows of tube banks. The study is performed using hot wire anemometry technique in an aerodynamic channel as well as flow visualizations in a water channel. In the wind channel three tube banks with square arrangement and pitch to diameter ratios $P/D = 1.26$, 1.4 and 1.6 were studied. The Reynolds number range for the velocities measurements, computed with the tube diameter and the flow velocity in the narrow gap between tubes was 7×10^4–8×10^4. Continuous and discrete wavelets were applied to decompose the velocity results, thus allowing the analysis of phenomena in time–frequency domain. Visualizations in a water channel complemented the analysis of the hot wire results. For this purpose, dye was injected in the flow in the water channel with a tube bank with $P/D = 1.26$. The range of the Reynolds number of the experiments was 3×10^4–4×10^4. The main results show the presence of instabilities, generated after the second row of the tube bank, which propagates to the interior of the bank. In the resulting flow, the three orthogonal components are equally significant. The three-dimensional behavior of the flow is responsible for a mass redistribution inside the bank that leads to velocity values not expected for the studied geometry, according to the known literature. The resulting flow process can be interpreted as a secondary flow which is characteristic of tube banks.

1. Introduction

Banks of tubes or rods are the most common approach to the study of the flow in shell-and-tube heat exchangers, found in nuclear and process industries. Attempts to increase heat exchange ratios in heat transfer equipments do not consider, as a priority of project criteria, structural effects caused by the turbulent fluid flow, unless failures occur (Païdoussis, 1982). By attempting to improve the heat transfer process, dynamic loads are increased and may produce vibration of the structures, leading, generally, to fatigue cracks and fretting-wear damage of the components, which are one of the failure sources affecting nuclear power plant performance (Pettigrew et al., 1998).

The concern about the integrity of heat transfer equipments is, therefore, due to the close relationship between fluid flow around a solid surface and the vibrations induced by the flow in the structure by wall pressure fluctuations. Ziada (2006) makes a comprehensive analysis using spectral tools and visualizations for several tube bank geometries where the classical results are summarized. For in-line tube arrays, he concludes that this geometry is dominated by symmetric instability of the jets issuing between the tube columns. This mode of vortex shedding persists on the whole depth of intermediate tube arrays. As the tube spacing is reduced, the jet instability and the spatial correlations are weakened.

By means of hot wire and pressure transducer measurements and Fourier analysis, Endres and Möller (2001), made a comprehensive study of velocity and pressure fluctuations in triangular and square arrangements. The results of spectra of velocity fluctuations in both tube banks with $P/D = 1.60$ show the presence of small peaks at Str = 0.21, which coincide with the value expected for vortex shedding in the case of a single cylinder. The peak is pronounced only in the tube bank with triangular arrangement. By reducing the P/D-ratio, the turbulence structure is reduced. In the range of 1.60–1.16, the energy of velocity fluctuations with small scales (large Strouhal numbers) is increased as P/D is reduced, while the highest values of cross-correlations between velocity and pressure fluctuations were found at $P/D = 1.26$.

The Fourier analysis employed in the above studies gives information about the frequencies involved and the interdependence

* Corresponding author. Tel.: +55 51 3308 3228; fax: +55 51 3308 3228.
E-mail address: svmoller@ufrgs.br (S.V. Möller).
[1] Present address: Fundação Universidade do Rio Grande - FURG, Rio Grande, RS, Brazil.
[2] Present address: Universidade do Vale do Rio dos Sinos - UNISINOS, São Leopoldo, RS, Brazil.

0029-5493/$ – see front matter © 2009 Elsevier B.V. All rights reserved.
doi:10.1016/j.nucengdes.2009.05.017

Nomenclature

a, b	wavelet parameters
$c(J, k)$	wavelet series of approximation coefficients
$d(j, k)$	wavelet series of detail coefficients
D	diameter (m)
f	frequency (Hz)
Fs	sampling frequency (Hz)
j, k	indexes
J	index of the last decomposition of a wavelet
P	pitch (m)
$P_{xx}(a, b)$	wavelet spectrum (m^2/s^2)
Re	Reynolds number ($U_{gap}D/\nu$)
Str	Strouhal number (fD/U_{gap})
t	time (s)
U_{ref}	reference velocity (m/s)
U_{gap}	gap velocity (m/s)
$x(t)$	generic function in time domain
$\tilde{X}(a, b)$	generic function in wavelet domain (continuous)
$\phi(t)$	generic scale function
$\Psi(t)$	generic wavelet function
CWT	continuous wavelet transform
DWT	discrete wavelet transform

of simultaneous phenomena like velocity and pressure fluctuations. In this case, the flow must be in steady state. In time varying series, Fourier analysis cannot be used. Furthermore, many processes of interest in fluid dynamics are not stationary. Indrusiak et al. (2005) explored the use of wavelets in the study of accelerating and decelerating flows through tube banks. In that study, hot wire measurements of flow velocities in two different gaps after one tube of the third row of the bank showed an intermittent behavior similar to bistable mode found for tubes placed side-by-side.

Olinto et al. (2006) compare the results obtained with hot wire measurements in a tube bank with square arrangement and $P/D = 1.26$ to the bistable flow from two cylinders side-by-side. The results show that, the highly disordered flow after the second and third rows influences the flopping process. In some configurations, the flopping does not allow the observation of a characteristic frequency, although evidencing the presence of vortex shedding. If the wake interaction occurs, as for two tubes placed side-by-side, the flopping is strongly influenced by the presence of the tubes of the next row. However, there is no space for the flopping formation as in the wake of two tubes or a single row of tubes. The consequence is that the flopped flow will be directed up or downwards, parallel to the tubes axes, giving a strong three-dimensional characteristic to the flow through tube banks.

The purpose of this paper is to deepen the study about the nonstationary wakes in the flow perpendicular to tube banks and discuss its relation with the bistable flow that occurs in some circular cylinder arrays, like side-by-side arrangements. With this purpose, wavelet analysis of velocity time series obtained through hot wire and flow visualizations are used to investigate the presence of a velocity component parallel to the tube axes.

2. Background

2.1. The bistable phenomenon

The bistable phenomenon occurs when a cross-steady flow impinges on a circular cylinders array with certain characteristics (Sumner et al., 1999). The circular cylinders should be side-by-side and the transversal pitch to diameter ratio (P/D) must be between 1.2 and 2.0. In this case, the flow is characterized by the presence of a narrow near-wake behind one of the cylinders and a wide near-wake behind the other, which generate two dominant vortex-shedding frequencies: the higher associated with the narrow wake and the lower with the wide wake. The gap flow deviates towards the cylinder with the narrow wake. In some cases, when the bistable phenomenon is present, the biased gap flow switches from one side to the other at irregular intervals of time. This pattern is independent of the Reynolds number, and it is not caused by cylinder misalignment or another external factor, but is an actual feature of the flow. Fig. 1 shows schemes of the bistable flow modes after two cylinders side-by-side and the effect on the velocity values due to the changing of flow modes.

According to Kim and Durbin (1988) the transition between the two asymmetric states is completely random and it is not associated with a natural frequency. The mean time interval between the transitions decreases as the Reynolds number increases.

Guillaume and LaRue (1999) classified the bistable regime according to its behavior:

- Quasi-stable behavior: different modes do not wary with time unless a large perturbation causes the change. The new situation is also stable.
- Spontaneous flopping: the average values alternate over the time between relatively high and low values.
- Forced flopping: the initially stable wakes exhibit flopping as a result of a large, one-time perturbation. After that, there is no difference between forced and spontaneous flopping.

Zdravkovich (1977) studied the side-by-side tubes geometry and found that, associated to the wakes, there are two different drag coefficients and the base pressure switches between two extreme values.

Zdravkovich and Stonebanks (2000) studied the wake behind a tube row and concluded that it is formed by coalescent jet cells that suddenly change their pattern. This state, which they defined as metastable, can be due to the rearrangement of the cell pattern

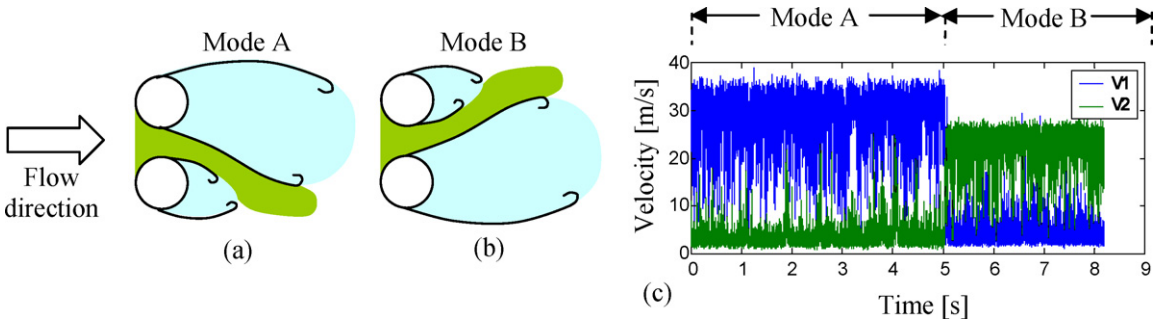

Fig. 1. Bistability flow modes after two cylinders side-by-side (a and b) and velocities at the wake (c).

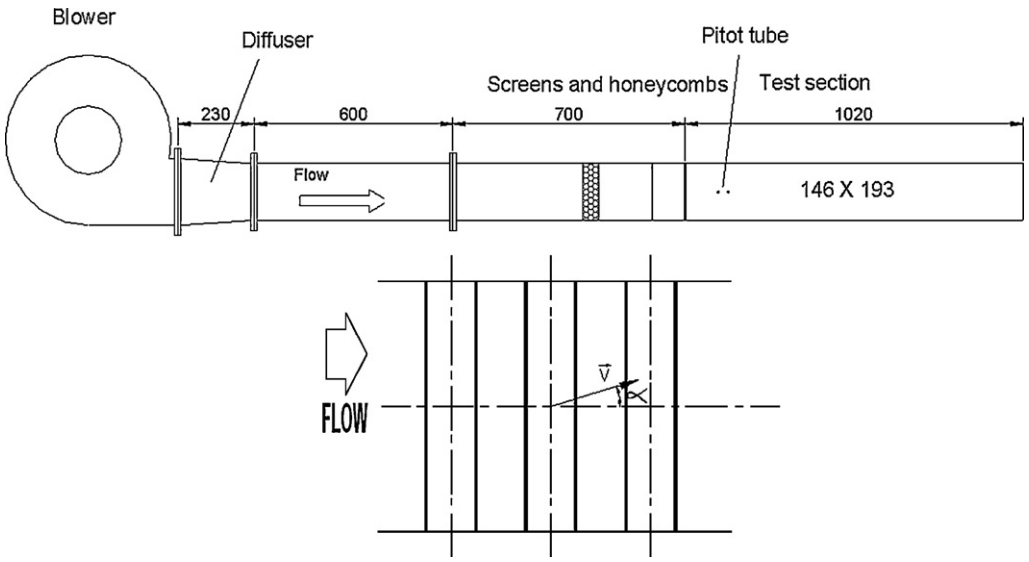

Fig. 2. Schematic view of the aerodynamic channel. Detail: tube bank with representation of flow velocity angle.

behind the row and is dependent on the number of tubes in the row.

Le Gal et al. (1996) also studied the flow through a tube row. For P/D values greater than 2, they found an identical and anti-phase vortex shedding. Conversely, when the P/D-ratio is less than 2, the jets between the tubes are deviated and the wake merges to form clusters. If the flow velocity is increased quickly from rest, several different patterns can be formed.

Alam et al. (2003) investigated experimentally the flow through two cylinders placed side-by-side for $Re = 5.5 \times 10^4$. They found, for intermediate P/D-ratios (1.2–2.2), the biased bistable regime. Using wavelet transforms, they showed that, when a mode switch occurs, an intermediate frequency might be present.

2.2. Fourier and wavelet transforms

The Fourier transform of a discrete time series gives the energy distribution of the signal in the frequency domain evaluated over the entire time interval.

While the Fourier transform uses trigonometric functions as basis, the bases of wavelet transforms are functions named wavelets, with finite energy and zero average that generates a set of wavelet basis.

The continuous wavelet transform of a function $x(t)$ is given by:

$$\tilde{X}(a,b) = \int_{-\infty}^{\infty} x(t)\psi_{a,b}(t)\ dt \tag{1}$$

where ψ is the wavelet function and the parameters a and b are respectively scale and position coefficients ($a, b \in \Re$) and $a > 0$.

The respective wavelet spectrum is defined as:

$$P_{xx}(a,b) = \left|\tilde{X}(a,b)\right|^2 \tag{2}$$

In the wavelet spectrum, Eq. (5), the energy is related to each time and scale (or frequency) (Daubechies, 1992). This characteristic allows the representation of the distribution of the energy of the signal over time and frequency domains, called spectrogram.

The discrete wavelet transform (DWT) is a judicious subsampling of the continuous wavelet transform (CWT), dealing with dyadic scales, and given by Percival and Walden (2000):

$$d(j,k) = \sum_t x(t)\psi_{j,k}(t) \tag{3}$$

where the scale and position coefficients ($j, k \in \mathrm{I}$) are dyadic subsamples of (a, b).

Any discrete time series with sampling frequency Fs can be represented by:

$$x(t) = \sum_k c(J,k)\phi_{J,k}(t) + \sum_{j \le J}\sum_k d(j,k)\psi_{j,k}(t) \tag{4}$$

where the first term is the approximation of the signal at the scale J, which corresponds to the frequency interval $[0, Fs/2^{J+1}]$ and the inner summation of the second term are details of the signal at the scales j ($1 \le j \le J$), which corresponds to frequency intervals $[Fs/2^{j+1}, Fs/2^j]$.

The velocity signals were analyzed using wavelet transforms to obtain the energy distribution of the turbulent flow over time–frequency domain. The continuous wavelet spectrum was obtained through continuous wavelet transform. The discrete wavelet transform was used to decompose the measured signal in wavelet approximations divided in frequency bands (Indrusiak et al., 2005). Mathematical tools were developed using the Matlab® software.

3. Experimental technique

3.1. Aerodynamic channel

The test section is the same used in Endres and Möller (2001), being a 2320 mm long rectangular channel, with 146 mm height and a maximal width of 193 mm, Fig. 2. Air, at room temperature, is the working fluid, driven by a centrifugal blower, passed by a diffuser and a set of honeycombs and screens, before reaching measurement location with about 1% turbulence intensity. After the screens, a Pitot tube was placed at a fixed position to measure the reference velocity for the experiments, used also for the calculation of the gap velocity for the determination of the Reynolds number of the experiments.

Measurements of velocity and velocity fluctuations were performed using a DANTEC *StreamLine* constant temperature hot wire anemometer. Single and double hot wire probes were used. Single

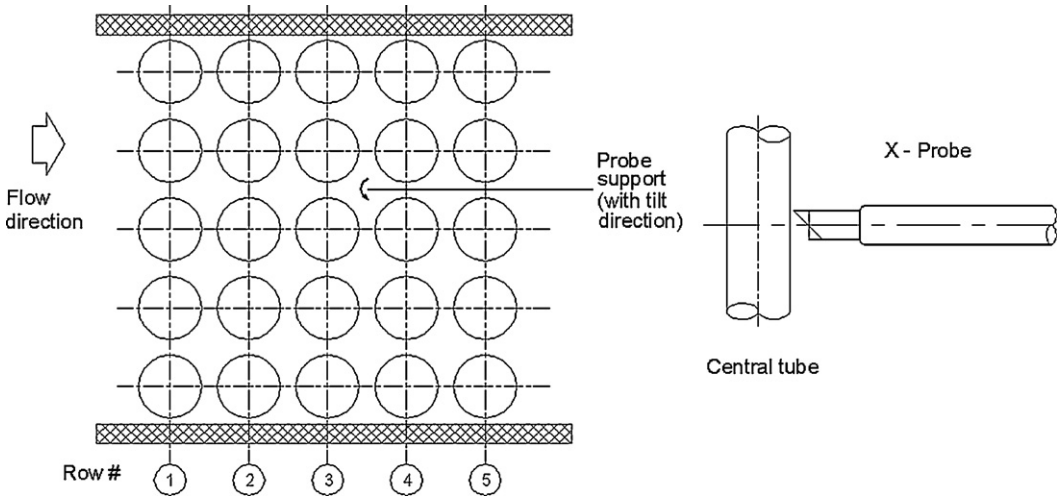

Fig. 3. Scheme of the tube bank with hot wire probe location.

probes had one wire perpendicular to the main flow. The double wire probe had one wire perpendicular to the main flow and a second wire inclined 45° to the main flow to allow simultaneous measurement of two components of the velocity and velocity fluctuations. The angle (α) between velocity vector and main flow direction in a plane parallel to tube axes was also determined (Fig. 2). To determine the measurement location, the probes were inserted in the bank and located in the center of the wide region between third and fourth rows, as shown schematically in Fig. 3, then slightly tilted in the direction of the central tube line. With the help of an oscilloscope, the raise in the amplitudes of the measured velocity characterizing the edge of the wake was determined.

The tube banks investigated had square arrangement and three different pitch-to-diameter ratios (P/D): 1.26, 1.4 and 1.6. The tubes had a diameter of 32 mm. They were rigidly mounted inside the channel. The flow was perpendicular to the tube axes. Data acquisition of instantaneous velocity was performed with a 12-bit Keithley DAS-58 A/D-converter board. The sample frequency was 3 kHz and a low pass filter set at 1 kHz was used.

3.2. Water channel and visualization technique

Several flow visualization techniques have being used for the turbulent flow study on tube banks. Sumner et al. (1999) used the Particle Image Velocimetry (PIV) technique and dye injection in order to visualize the flow through two and three tube arrangements. Williamson (1985) employed the smoke injection inside a wind channel to visualize the generation modes and vortex shedding on a bluff body pair for several Reynolds numbers. Le Gal et al. (1996) employed hydroxyl smoke, to visualize the flow, downstream to the wakes of a tube row. Guillaume and LaRue (1999) used smoke injection, lightened by a laser plane to visualize the bistable regime in tube arrangements with two or three tubes. This technique was also used by Zhang and Zhou (2001) to study the unlike spacing effect on the vortex shedding in arrangements with three cylinders placed side-by-side, and by Xu et al. (2003) to study the Reynolds number effect on the flow structure behind two side-by-side tubes. Hiramoto and Higuchi (2003) employed the hydrogen bubble technique to visualize the flow and Digital Particle Image Velocimetry (DPIV) to make measurements of the velocity field in the vortex shedding behind a pair of cylinders. Alam et al. (2003) also employed the hydrogen bubbles technique to study the flow through tube arrangements. Dye was employed by Ziada et al. (1989), Ziada and Oengören (1992, 1993), Oengören and Ziada (1992, 1998) and Ziada (2000).

In this work, the visualization experiments were performed in a water channel facility of the Hydraulic Research Institute - IPH/UFRGS. The water channel has a settling chamber with a honeycomb which acts as a flow straightener, a nozzle, a 30 m long open channel (10 m upstream, 20 m downstream the test section) with 0.5 m × 0.6 m rectangular cross-section, a vertical gage to control the water level, and a discharge tank with the return pipe to close the circuit. The flow rate is read by an electromagnetic flowmeter and can vary from 0.0006 to 0.22 m^3/s, resulting in velocities from 3×10^{-3} to 1.1 m/s. The maximum flow depth is 0.5 m which is controlled through the flow rate, by a set of valves in the feeding pipeline, and by the vertical gage placed in the discharge.

The tube bank used for the visualizations had a square arrangement, being a 2.34:1 scale model of the bank with same $P/D = 1.26$ studied in the aerodynamic channel. The bank was made from commercial PVC tubes with diameter of 75 mm, with exception of the central tube, which was made using a translucent acrylic glass tube. A mirror was fixed inside this tube at the mid-height of the channel, inclined 45° with the tube axis direction to allow the visualization of a dye thread injected from a hole on the wall of the neighboring tube. The tubes were fixed vertically in a translucent acrylic glass test section. The water level was maintained about 60 mm above the test section upper wall, to avoid the effect of the gravitational waves at the free surface of the water.

Dye was injected by three procedures (labeled 1, 2 and 3 in Fig. 4): in the first one, four needles injected the dye aligned with the longitudinal gap between two tube lines, 60 mm below the top wall of the test section. In the second procedure, the dye was injected through a hole on the wall of the tube adjacent to the acrylic glass tube in the same row and is visualized through the mirror. This arrangement allows the viewing of the flow inside the tube bank, especially at the vertical plane. A detail of the tube with the inclined mirror and the location of the ink tap, procedure #2, is shown in Fig. 5, for a single tube row. In the third procedure, dye injection through a needle located upstream the tube bank, 60 mm above the bottom, enabled the visualization of the flow in the horizontal plan near the bottom of the test section. In all procedures, dye was gravity forced.

4. Results

4.1. Velocity measurements

Fig. 6 shows plots of velocity modulus and the angle formed by the velocity vector and the channel axis (α) measured at a loca-

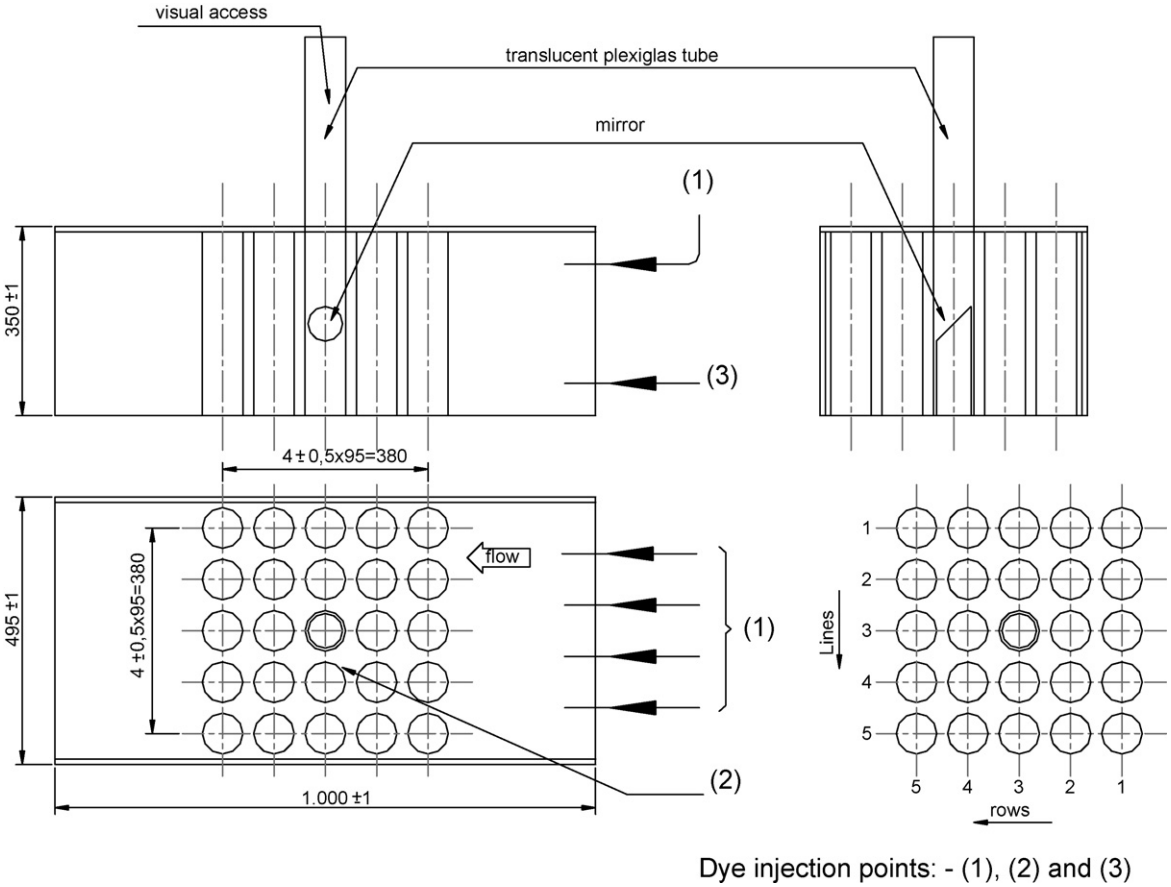

Fig. 4. Dimensional scheme of the test section for the flow visualization experiments.

tion behind the center tube of the third row in the tube bank with $P/D = 1.26$. The Reynolds number, calculated with the gap velocity and the tube diameter was 8.4×10^4. The angle is measured in a vertical plane, considering positive values when the incident velocity on the probe is upwards. A detail from the time interval from 3 to 5 s, Fig. 7, allows the identification of some patterns in the signals, not visible in Fig. 6, that occur and remain during some time, then changing to a new pattern. In the quoted case, from 4.15 to 4.3 s and 4.4 to 4.55 s a reduction in the velocity fluctuation occurs while the mean velocity value stays about 30 m/s. In the same time interval, the fluctuation of the incident angle decreases and the mean value is about 20°. The same pattern occurs from 3.2 to 3.3 s and other intervals less clearly. At the interval between 3.5 and 3.8 s, the behavior is opposite, the velocity fluctuates around 10 m/s while the incident angle has large range of fluctuation.

For a better observation of this process, the wavelet discrete transform can decompose velocity and angle signals in frequency bands, Fig. 8. The mean value of the velocity is given by the first approximation, from 0 to 2.9 Hz. In the interval between 4.2 and 4.6 s, the mean velocity stays around 25 m/s, modulated by a frequency between 2.9 and 5.8 Hz that causes the fall in the instantaneous velocity at the time location 4.5 s, shown in Fig. 7. At the

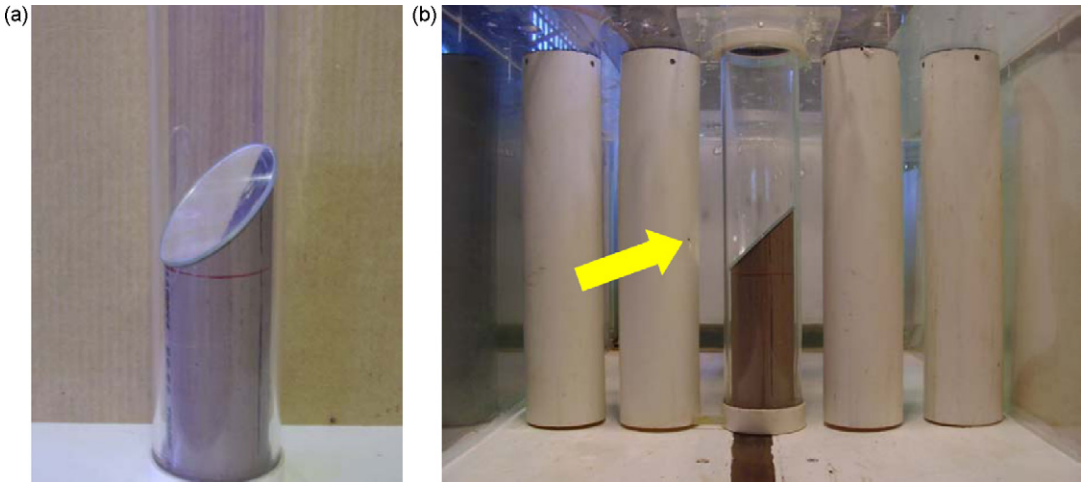

Fig. 5. Detail of the central tube with the mirror (a) and the central tube in a tube row—arrow shows location of ink injection tap on the neighboring tube wall (b).

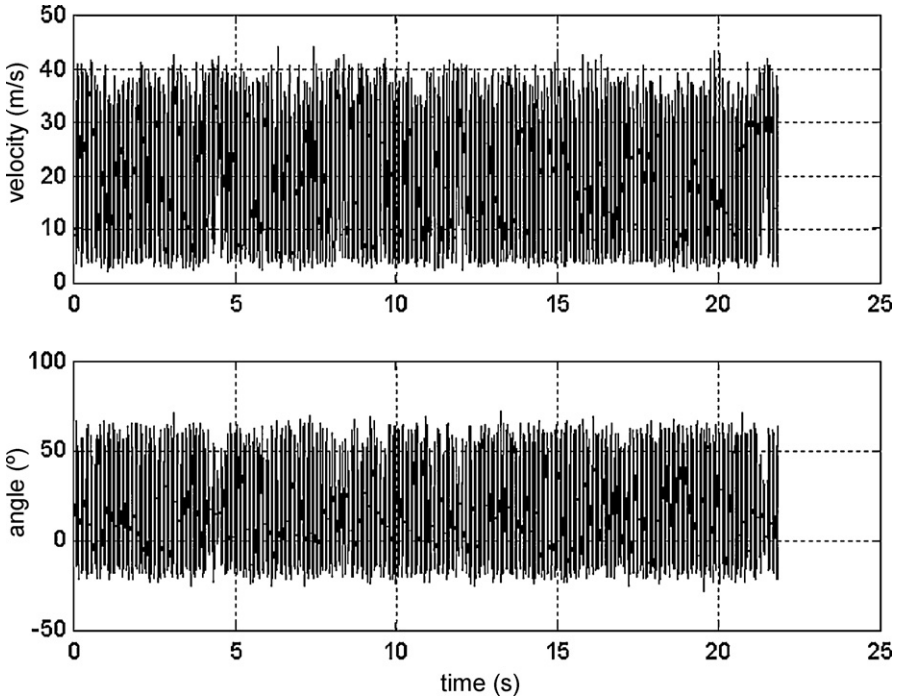

Fig. 6. Velocity and incident angle measured behind the center tube of the third row ($P/D = 1.26$).

interval between 3.5 and 3.8 s, the velocity has values about 15 m/s. When the velocity values increase, the higher frequency bands have lower amplitude. Conversely, when the velocity values decrease, the higher frequencies bands have higher amplitude.

The incident angle changes associated with the velocity values. When the velocity has a high value, the incident angle is low, and the velocity vector aligned with the channel axis. For the lowest velocities, the angle fluctuations are the largest for all frequency bands.

Fig. 9a and b presents the spectrograms of the signals from Fig. 8a and b, respectively. In Fig. 9a, the spectrogram of the velocity signal shows that, when the velocity fluctuates around the higher values, there is an energy concentration on the lower frequencies (3–3.3 s and 4.2–4.6 s). On the other hand, in the interval where the velocity fluctuates around the lowest velocity values, there is an energy spread on several frequencies (3.4–4.2 s).

The incident angle spectrogram (Fig. 9b) presents a similar behavior. For the higher velocity values, the incident angle has the

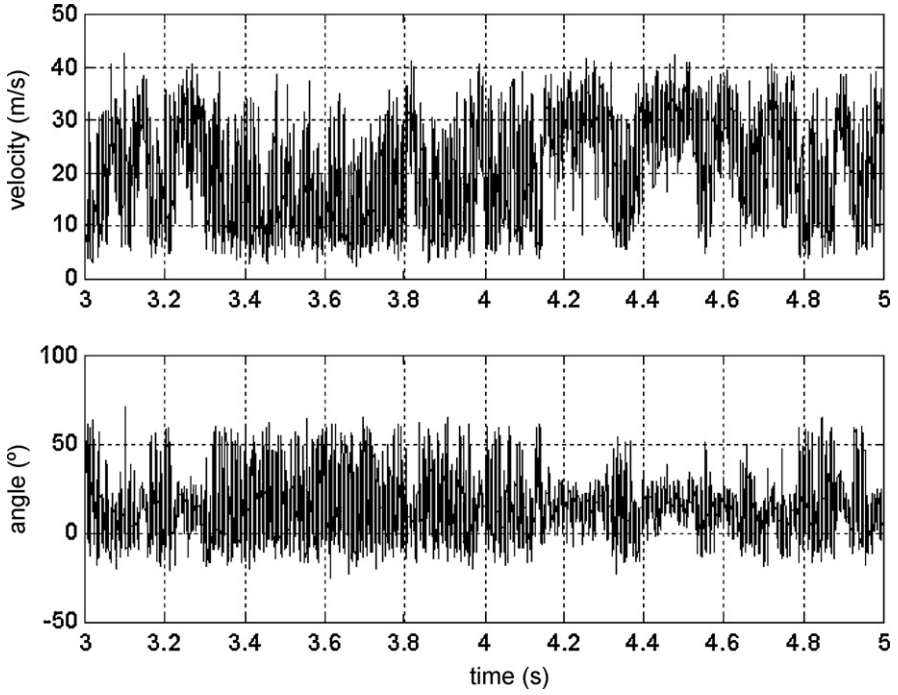

Fig. 7. Detail of velocity and incident angle measured behind the center tube of the third row from 3 to 5 s ($P/D = 1.26$). See Fig. 7.

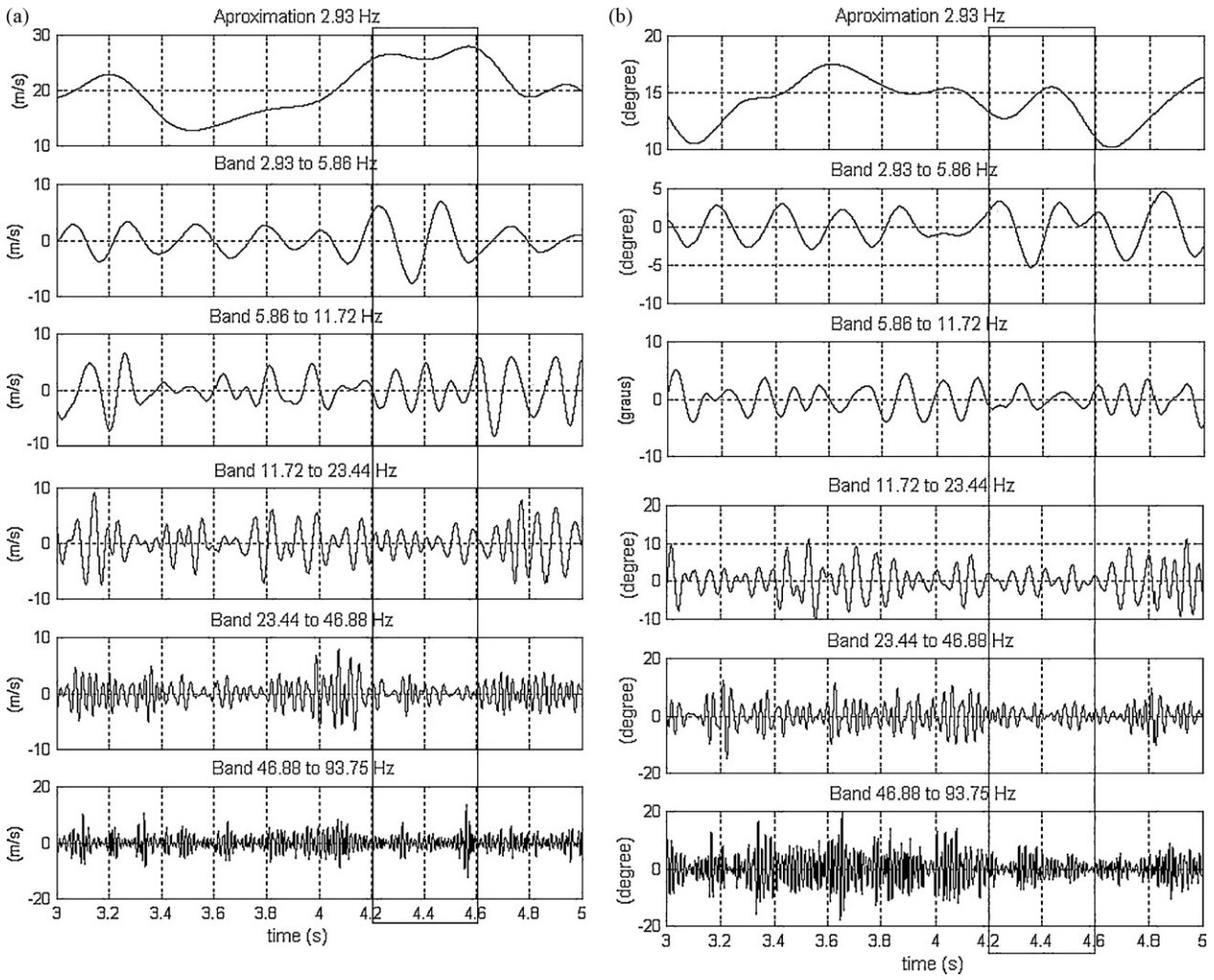

Fig. 8. Velocity (a) and incident angle (b) decomposition in frequency bands, using discrete wavelet transform of signals presented in Fig. 7. Tube bank with $P/D = 1.26$.

lower fluctuation energy for all frequency bands (4.2–4.6 s). It can also be observed in this diagram that, when the velocity is low, the energy is scattered for all frequencies (3.4–4.2 s).

The second tube bank investigated in the aerodynamic channel had $P/D = 1.4$. The Reynolds number was 7.4×10^4. The characteristics of instantaneous velocity and incident angle signals in this case are similar to those found for the tube bank with $P/D = 1.26$, associating an increase in the velocity to a decrease of the incident angle fluctuations (e.g. 6.5–8 s and 12–13 s), Fig. 10.

The decomposition in frequency bands, likewise the tube bank with $P/D = 1.26$, demonstrated that, when the velocity increases (e.g. from 6.5 to 8 s and from 12 to 13 s), the velocity fluctuation in higher frequency bands decreases. Besides, when the velocity remains at higher values, the values of the incident angle are low, with low fluctuations. In this geometry, the shift between the flow modes does not occur in characteristic time intervals.

The next experiment was made using the tube bank with $P/D = 1.6$ and the velocity and incident angle series obtained behind the third row. The Reynolds number was 7.4×10^4. The simultaneous signals are shown in Fig. 11.

Fig. 12a and b shows velocity and incident angle decomposition in frequency bands. In this series, it is possible to identify the presence of two different flow modes in the instantaneous velocity and incident angle signals. The shifts between these modes occur seven times during the time interval. In the velocity signal decomposition, associated to the interval where the velocity remains at higher values (~28 m/s), the fluctuation amplitude, for all frequency bands, have the lower values. On the other hand, when the velocity fluctuates around the lower values (~17 m/s), the larger frequency fluctuations are present. In the incident angle decomposition, a sim-

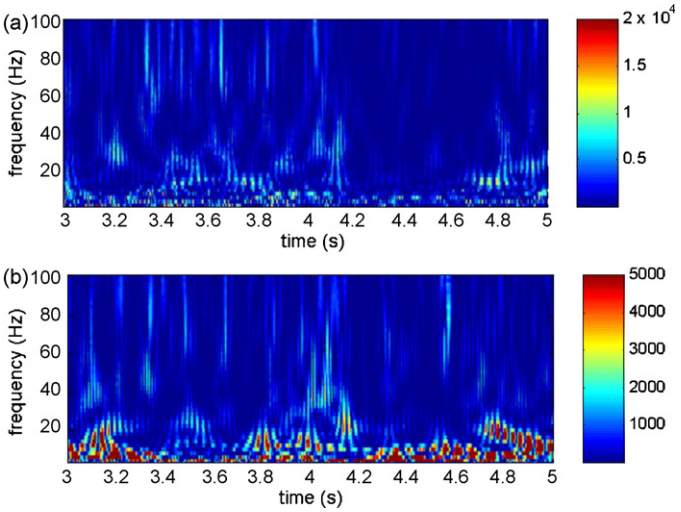

Fig. 9. Spectrogram of velocity (a) and velocity incident angle (b) for the signal presented in Fig. 7 (bar indicates the arbitrary energy scale used).

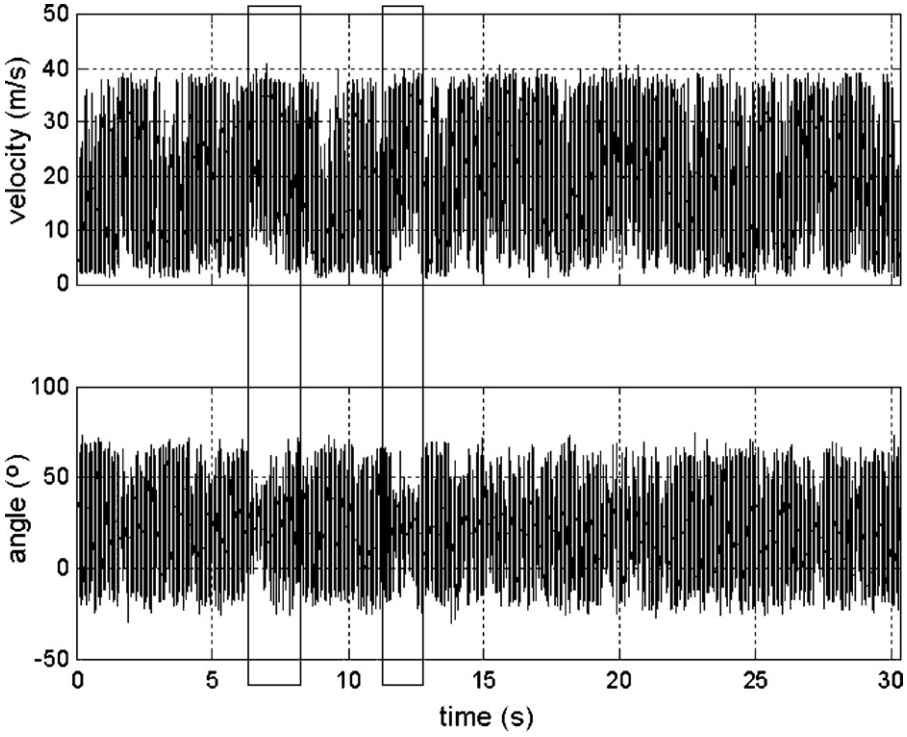

Fig. 10. Velocity and incident angle measured behind the central tube at the third row ($P/D = 1.4$).

ilar behavior is found. During the time intervals where the mean angle tends to stabilize around 11°, there is a reduction in the fluctuation amplitude, for all frequency bands, especially for higher frequencies.

Fig. 13 presents the spectrogram obtained with the continuous wavelet transform for the interval from 44 to 76 s. In this time interval, the flow mode shift occurs at about 60 s. Before 60 s, the energy is scattered over all frequencies presented. After this time, the spectrogram presents low energy values for all frequencies, confirming the lower fluctuations at the highest velocities.

These results are rather inconclusive. It is clear that the changing phenomena, alternating high velocity values accompanied by low values of the incident angle and low velocity values with high fluctuations of the incident angle, cannot be explained directly from the measurements. A three-dimensional characteristic of the flow is expected, but the flow features were not

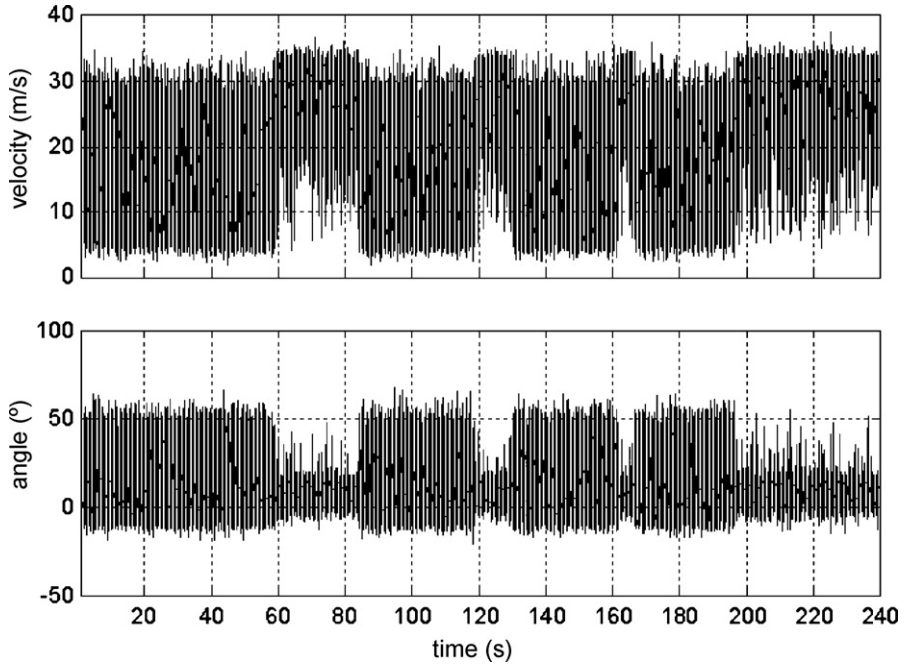

Fig. 11. Velocity and incident angle measured behind the third row for tube bank with $P/D = 1.6$.

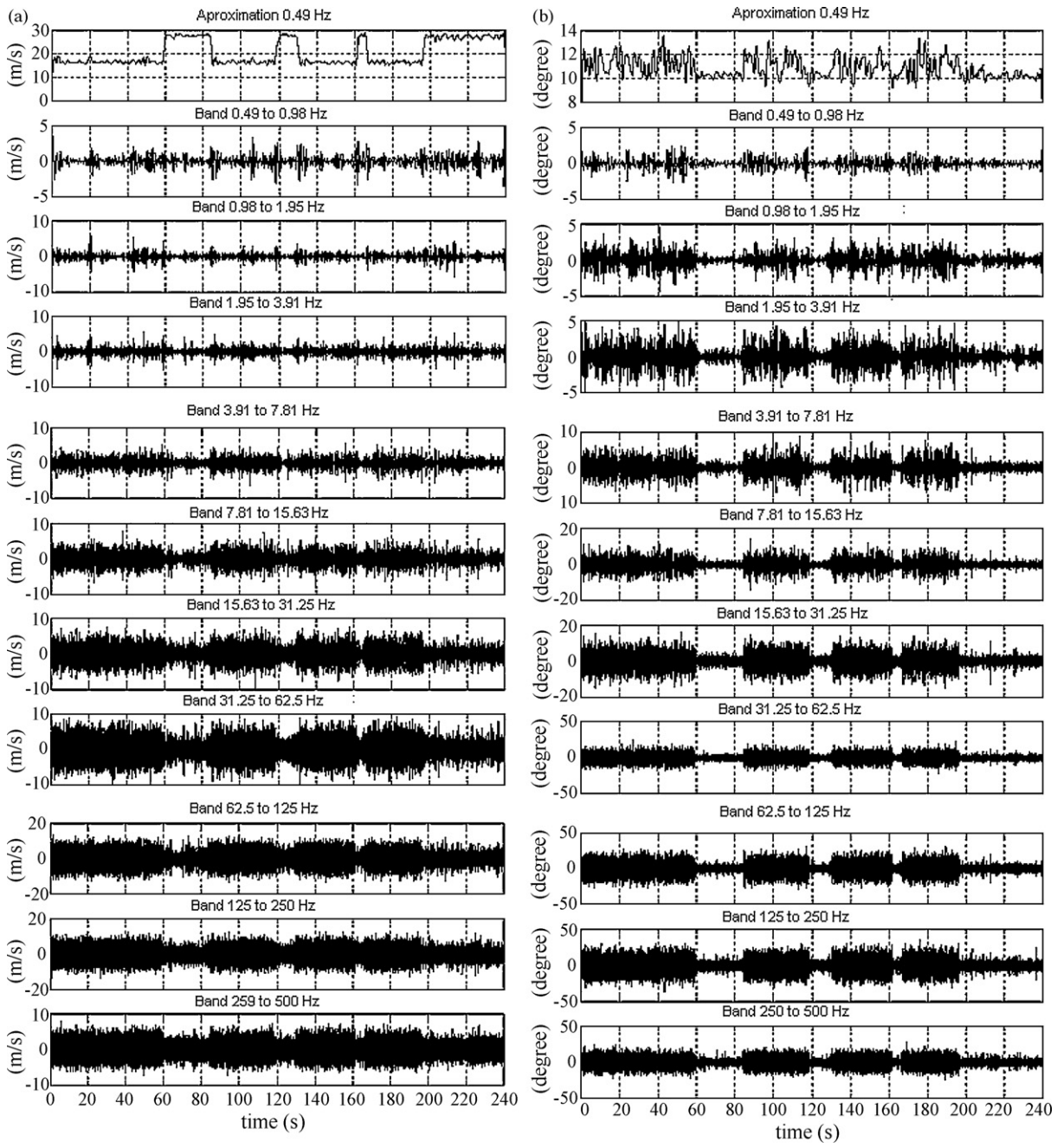

Fig. 12. Velocity (a) and incident angle (b) decomposition of signal in Fig. 11 in frequency bands, using wavelet discrete transform. Tube bank with $P/D = 1.6$.

obtained from the analysis of velocity and incident angle. Flow visualizations can contribute for the interpretation of the results above.

4.2. Flow visualizations

In the water channel, dye was injected 270 mm upstream of the first row and from a hole on the wall of the central tube at the third row, as indicated in Figs. 4 and 5.

Fig. 14 shows the visualization of the flow impinging on two cylinders side-by-side and on a single row of cylinders. In the row of cylinders the wide wake spreads to both sides, while in the case of two cylinders it is directed by the main flow to the rear of the neighboring cylinder. Concerning to Fig. 14a, it corresponds to the results presented in Fig. 1. The main difference between results from the aerodynamic channel and the water channel is that in the former the bistability, characterized by the flow mode change is present, while in the water channel, once a flow configuration is established it does not change, unless the flow is completely stopped and restarted again.

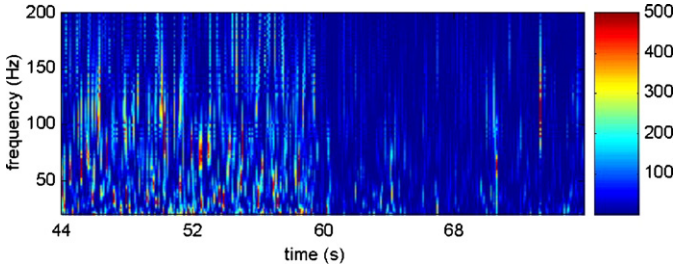

Fig. 13. Spectrogram of part of velocity signal—between 44 and 76 s ($P/D = 1.6$).

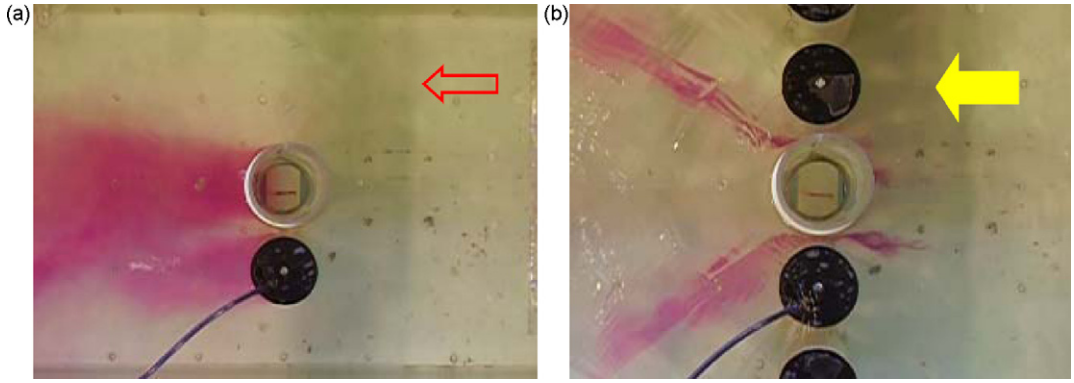

Fig. 14. Visualization of the flow on two cylinders side-by-side (a) and on a single row of cylinders (b). Flow direction from right to left.

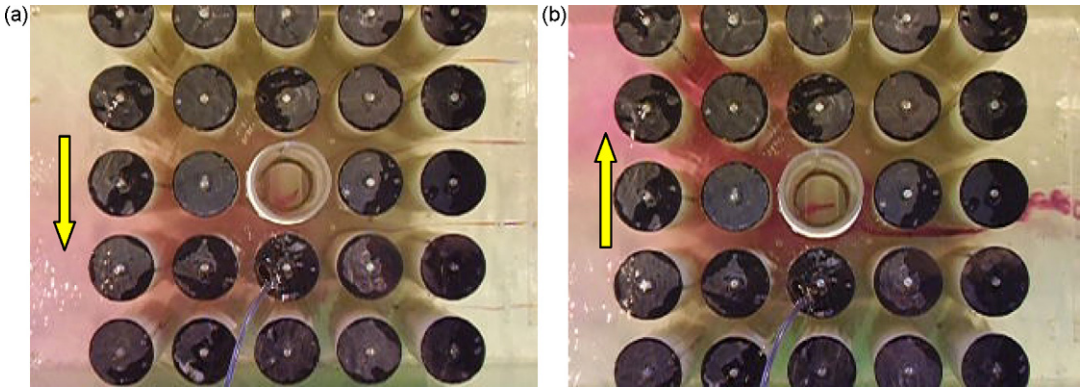

Fig. 15. Flow visualization in the tube bank with $P/D = 1.26$. $Re = 3.07 \times 10^4$. (a) Injection at 60 mm below upper wall and (b) injection at 60 mm above the bottom (arrows indicate direction of the deviation). Central tube: mirror shows flow deviation downwards. Main flow is from right to left.

In the experiment shown in Fig. 15, the flow close to the upper wall of the test section undergoes a deviation to the left, when viewed from upstream to downstream (Fig. 15a). Close to the bottom, the flow deviates to the right (Fig. 15b).

In a subsequent experiment, Fig. 16, an opposite flow pattern is present: the flow near the upper wall deviates to the right, whereas the flow near the bottom deviates to the left (when viewed from upstream to downstream).

In Figs. 15 and 16, the cases a and b correspond respectively to the dye injection points #1 and #3, shown in Fig. 4.

Fig. 17a and b shows details of the observations through the mirror in the experiments of Figs. 15 and 16, respectively. When the flow near the upper wall is deviated to the left (Fig. 15), the dye thread is deviated downwards, showing that the flow inside the bank is deviated downwards, Fig. 17a. In Fig. 17b, the flow is deviated upwards, corresponding to the case of Fig. 16, where the flow near the upper wall deviates to the right.

The results shown in Figs. 15–17 do not have differences in their experimental conditions. They just result from experiments made at different times.

In general, it was observed that the dye thread travels aligned with the channel axes until it reaches the bank, where it deviates strongly to one side (left or right), traveling and spreading in diagonal direction. The side of the deviation is constant for each run of the experiment but changes randomly from one run to another. This is different from the flow in the air channel, were the devia-

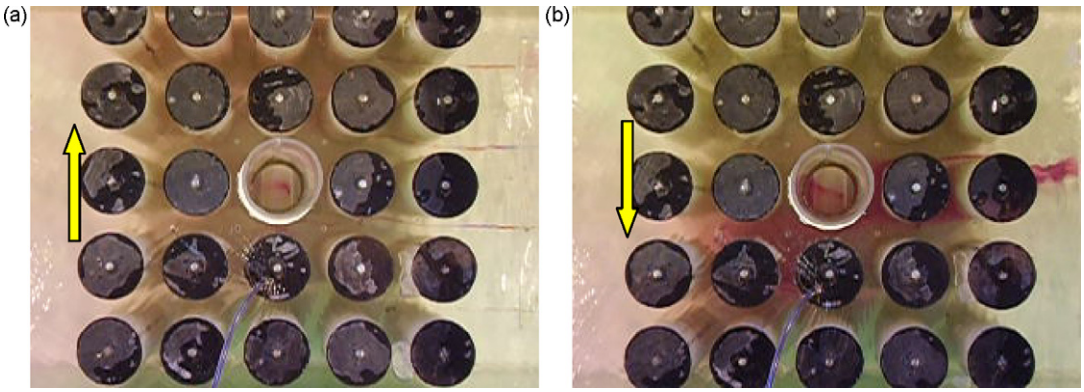

Fig. 16. Flow visualization in the tube bank with $P/D = 1.26$. $Re = 3.18 \times 104$. (a) Injection at 60 mm below upper wall and (b) injection at 60 mm above the bottom (arrows indicate direction of the deviation). Central tube: mirror shows flow deviation upwards. Main flow is from right to left.

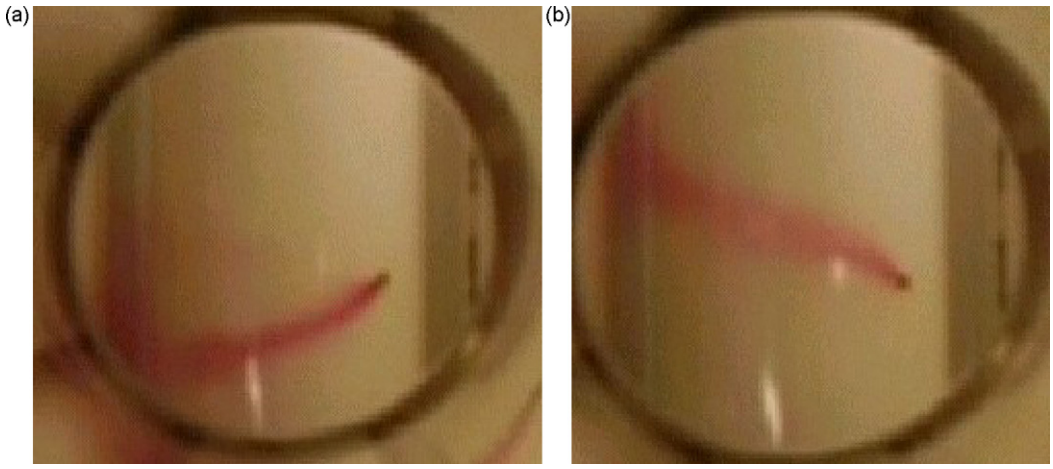

Fig. 17. Visualization of the dye flow on the tube surface through the mirror inside the acrylic glass tube: (a) downward flow-detail of Fig. 15 and (b) upward flow-detail of Fig. 16.

tion, observed by velocity changes in the hot wire signal, occurred randomly along time, during the measurements.

The visualizations described above evidence that in the study of turbulent flows through tube banks the three orthogonal flow components must be considered. They also confirm the behavior of the velocity vector measured after the third row, explaining the two modes described in the previous section.

5. Discussions and conclusions

In this work, an experimental study of the cross-flow in the first rows of tube banks with square arrangement is presented. In order to detect the instabilities generated in these first rows, velocity measurements were performed in an aerodynamic channel. The tube banks used had square arrangement and pitch to diameter ratios of 1.26, 1.4 and 1.6. Additionally, flow visualizations in a water channel in a tube bank with $P/D = 1.26$ allowed the interpretation of the experimental results obtained with hot wire anemometry.

A phenomenon of random change in the flow mode was identified, characterized by the presence of transversal components to the main flow that leads to the generation of three-dimensional behavior with the same scale to that of the channel. The occurrence of such phenomenon can become an important origin of dynamic instabilities, since it can alternate the lift and drag coefficients on the tubes, modifying the dynamic response of the involved structures.

The identified phenomenon is similar to the bistable flow that occurs in the flow on two tubes located side-by-side. Similar phenomenon also occurs in the flow on a tube row, where the wakes emerging from the narrow gap between the tubes, are turned aside to form unstable sets that can randomly change of configuration. The interaction of two or more wakes deflects the flow to one side or to the other, being able to remain in this position for some time and later reassuming its random behavior. This phenomenon has its origin in the velocity and neighboring wake fluctuations. In the beginning of the process, it is expected that the wakes are generated independently in the back side of each tube in the bank. If the neighboring vortices have the same phase, the fluctuation will cause the growth of the wake. If the P/D-ratio is sufficiently small to guarantee the interaction between the wakes of the adjacent tubes, the resulting wake will not behave like the one from a single bluff body, but rather is influenced by the flow through the gap between the tubes. Since there is no room for the formation of the wake, due to the presence of the tubes of the following row, a transversal component of the flow is generated and, at the same time that the flow is directed toward the next gap, it is directed up or downwards. From this process, a strong three-dimensional characteristic for the flow through the bank will result, as shown in Fig. 18, where a scheme of the flow visualization of Fig. 15 is presented. This flow process occurs in the plane formed by the axis of the tubes and the direction of the main flow causing a mass redistribution that generates a velocity component transversal to both the channel and tube axes. The scheme in Fig. 18 explains also the vertical flow component that is observed through the mirror in the acrylic tube (Fig. 17). The resulting flow will remain deviated behind the tube row, until a new disturbance breaks the stability and the process starts again.

Fig. 18 explains also the relation between velocity value and flow angle. When the angle between velocity vector and main channel axis is low, the velocity is high, that means that the main flow is parallel to the channel axis. When the angle is high (positive or negative), the flow in measurement location is deviated down or upwards. This is accompanied by a deviation to the left or right near the upper and lower walls. The resulting flow process can be interpreted as a secondary flow which is characteristic of tube banks.

However, in the water channel, once the flow is deviated to a certain direction it will remain unchanged along time. To obtain another flow configuration it is necessary to restart the process from the beginning.

Therefore, following Guillaume and LaRue (1999), the bistable process in tube banks can be classified as ‘spontaneous flopping’ in air and ‘quasi-stable’ in water.

Due to the changes in the flow direction, the resulting velocity inside of the several gaps of the tube bank is not homogeneously distributed. This velocity difference can cause vortex shedding in different frequencies throughout the bank.

The velocity measurements, performed in the three geometries of tube banks, resulted in different permanence times for each mode, depending on the pitch to diameter ratio. For the tube bank with $P/D = 1.26$, the time of permanence in each mode was of the order of 0.5 s. For the bank with $P/D = 1.4$ the mode changed within the range of 1–2 s and, for the bank with $P/D = 1.6$, it was around 10 s. This leads to conclude that the time duration of a certain flow mode is associated with the geometry of the tube bank. The larger the P/D-ratio, the longer will be the time of permanence in each flow mode.

The visualization experiments allowed the recognition that the beginning of this transversal flow occurs at the second row of the tube bank. In the experiments where air was the working fluid, the change in the flow mode occurred spontaneously, following a random characteristic. In the experiments of visualization in water

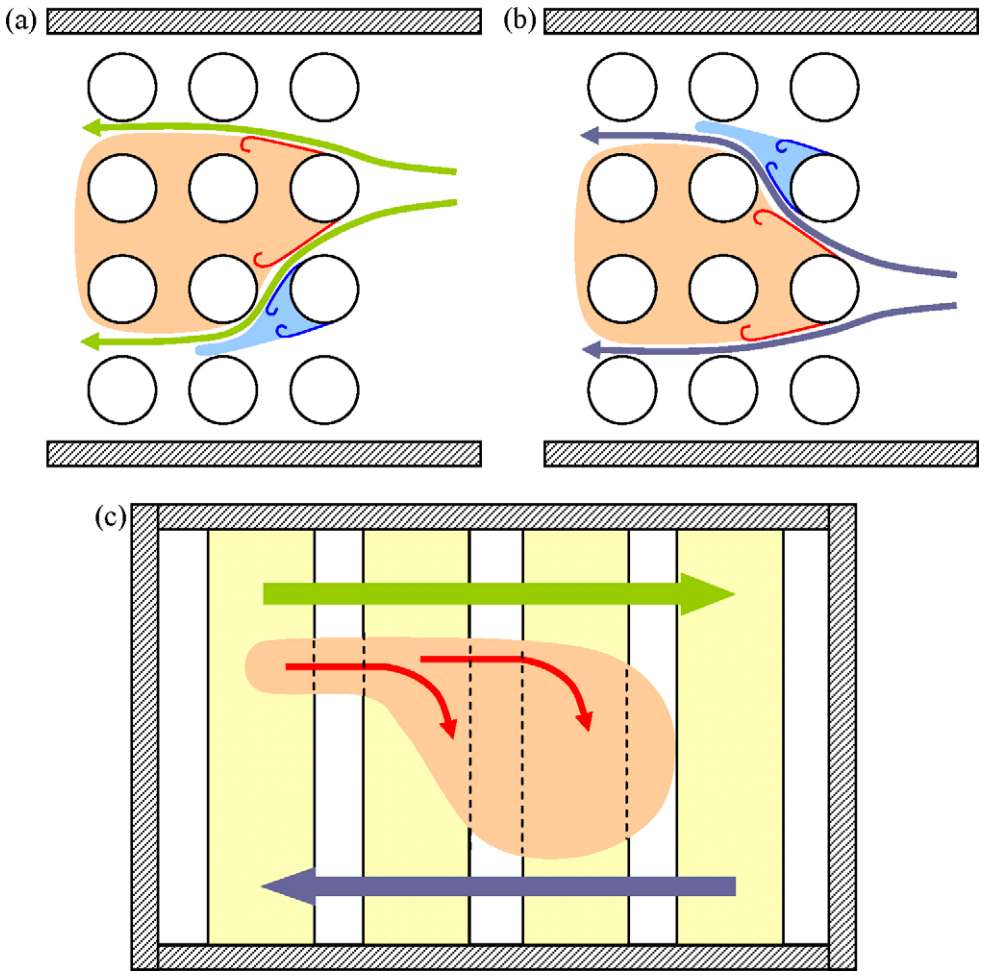

Fig. 18. Schematic representation of bistability process of Fig. 15: (a) near the upper wall; (b) near the bottom; (c) cross-section view of tube bank, showing the three-dimensional effect of the flow.

channel, this spontaneous mode change did not occur. The changes in the flow mode occurred only by stopping and then restarting the water circulation system. Similar fact was also cited by Sumner et al. (1999), where the bistable nature of the deviated flow was not detected in water channel. They attributed it to the combination of a small degree of misalignment of the cylinders and to experimental effects from the aspect and blockage ratios. Sumner et al. (1999) consider also the fact that previous experiments, in which the bistable flow pattern was reported, had been performed only in wind tunnels. This process, therefore, seems to be associated to the characteristics of the fluid and the channel geometric relations used in the studies. Future work will verify, through similarity study, if the classic dimensionless groups are able to capture all the characteristics of the studied flows.

The performed study, that allowed the identification of the three-dimensional effect generated in the first rows of tube banks, strengthens the idea that the two-dimensionality hypothesis used in some situations as a simplification in the analysis of tube banks, cannot consider important characteristics of the flow.

Acknowledgements

Authors are gratefully indebted to the CNPq - National Council for Scientific and Technological Development, for the financial support.

Cláudio R. Olinto thanks CAPES - Ministry of Education, Brazil, for granting him a fellowship (PICDT).

References

Alam, M.M., Moriya, M., Sakamoto, H., 2003. Aerodynamic characteristics of two side-by-side circular cylinders and application of wavelet analysis on the switching phenomenon. Journal of Fluids and Structures 18, 325–346.

Daubechies, I., 1992. Ten Lectures on Wavelets. Society for Industrial and Applied Mathematics.

Endres, L.A.M., Möller, S.V., 2001. On the fluctuating wall pressure field in tube banks. Nuclear Engineering and Design 203, 13–26.

Guillaume, D.W., LaRue, J.C., 1999. Investigation of the flopping regime with two-, three- and four-cylinder arrays. Experiments in Fluids 27, 145–156.

Hiramoto, R., Higuchi, H., 2003. Vortex shedding behind a non-parallel pair of circular cylinders. Journal of Fluids and Structures 18, 131–143.

Indrusiak, M.L.S., Olinto, C.R., Goulart, J.V., Möller, S.V., 2005. Wavelet time–frequency analysis of accelerating and decelerating flows in a tube bank. Nuclear Engineering and Design 235, 1875–1887.

Kim, H.J., Durbin, P.A., 1988. Investigation of the flow between a pair of circular cylinders in the flopping regime". Journal of Fluid Mechanics 196, 431–448.

Le Gal, P., Peschard, I., Chauve, M.P., Takeda, Y., 1996. Collective behaviour of wakes downstream a row of cylinders". Physics of Fluids 8, 2097–2106.

Oengören, A., Ziada, S., 1992. Vortex shedding and acoustic resonance in an in-line tube bundle. Part II. Acoustic resonance. Journal of Fluids and Structures 6, 293–309.

Oengören, A., Ziada, S., 1998. An in-depth study of vortex shedding, acoustic resonance and turbulent forces in normal triangle tube array. Journal of Fluids and Structures 12, 717–758.

Olinto, C.R., Indrusiak, M.L.S., Möller, S.V., 2006. Experimental study of the bistable flow in tube arrays. Journal of the Brazilian Society of Mechanical Sciences and Engineering XXVIII, 233–241.

Païdoussis, M.P., 1982. A review of flow-induced vibrations in reactors and reactor components. Nuclear Engineering and Design 74, 31–60.

Percival, D.B., Walden, A.T., 2000. Wavelet Methods for Time Series Analysis. Cambridge University Press.

Pettigrew, M.J., Taylor, C.E., Fisher, N.J., Yetisir, M., Smith, B.A.W., 1998. Flow-induced vibration: recent findings and open questions. Nuclear Engineering and Design 185 (2–3), 249–276.

Sumner, D., Wong, S.S.T., Price, S.J., Païdoussis, 1999. Fluid behaviour of side-by-side circular cylinders in steady cross-flow. Journal of Fluids and Structures 13, 309–338.
Williamson, C.H.K., 1985. Evolution of a single wake behind a pair of bluff bodies. Journal of Fluid Mechanics 159, 1–18.
Xu, S.J., Zhou, Y., So, R.M.C., 2003. Reynolds number effects on the flow structure behind two side-by-side cylinders". Physics of Fluids 15 (5), 1214–1219.
Zdravkovich, M.M., Stonebanks, K.L., 2000. Intrinsically non-uniform and metastable flow in and behind tube arrays. Journal of Fluids and Structures 4, 305–319.
Zdravkovich, M.M., 1977. Review of flow interference between two circular cylinders in various arrangements. Journal of Fluids Engineering (Transactions of the ASME) 99, 618–633.
Zhang, H.J., Zhou, Y., 2001. Effect of unequal cylinder spacing on vortex streets behind three side-by-side cylinders. Physics of Fluids 13 (12), 3675–3686.
Ziada, S., 2000. Flow periodicity and acoustic resonance in parallel triangle tube bundles. Journal of Fluids and Structures 14, 197–219.
Ziada, S., 2006. Vorticity shedding and acoustic resonance in tube bundles. Journal of the Brazilian Society of Mechanical Sciences and Engineering XXVIII, 186–199.
Ziada, S., Oengören, A., 1993. Vortex shedding in an in-line tube bundle with large tube spacing. Journal of Fluids and Structures 7, 661–687.
Ziada, S., Oengören, A., Bühlmann, E.T., 1989. On acoustical resonance in tube arrays. Part I. Experiments. Journal of Fluids and Structures 3, 293–314.
Ziada, S., Oengören, A., 1992. Vortex shedding and acoustical resonance in an in-line tube bundle. Part I. Vorticity shedding. Journal of Fluids and Structures 6, 271–292.